NAVAL POSTGRADUATE SCHOOL

Monterey, California

THESIS

CORRELATION BETWEEN SATELLITE-DERIVED
AEROSOL CHARACTERISTICS AND
OCEANIC DIMETHYLSULFIDE (DMS)

by

Richard A. Shema

December 1988

Thesis Advisor: P. A. Durkee

Approved for public release; distribution is unlimited.

REPORT DOCUMENTATION PAGE

Form Approved OMB No. 0704-0188

1a REPORT SECURITY CLASSIFICATION UNCLASSIFIED	1b RESTRICTIVE MARKINGS
2a SECURITY CLASSIFICATION AUTHORITY	3 DISTRIBUTION/AVAILABILITY OF REPORT Approved for public release; distribution is unlimited.
2b DECLASSIFICATION/DOWNGRADING SCHEDULE	
4 PERFORMING ORGANIZATION REPORT NUMBER(S)	5 MONITORING ORGANIZATION REPORT NUMBER(S)

6a NAME OF PERFORMING ORGANIZATION Naval Postgraduate School	6b OFFICE SYMBOL (If applicable) Code 63	7a NAME OF MONITORING ORGANIZATION Naval Postgraduate School	
6c ADDRESS (City, State, and ZIP Code) Monterey, CA 93943-5000		7b ADDRESS (City, State, and ZIP Code) Monterey, CA 93943-5000	
8a NAME OF FUNDING/SPONSORING ORGANIZATION	8b OFFICE SYMBOL (If applicable)	9 PROCUREMENT INSTRUMENT IDENTIFICATION NUMBER	
8c ADDRESS (City, State, and ZIP Code)		10 SOURCE OF FUNDING NUMBERS	
		PROGRAM ELEMENT NO.	PROJECT NO.
			TASK NO.
			WORK UNIT ACCESSION NO.

11 TITLE (Include Security Classification)
CORRELATION ~~OF~~ SATELLITE-~~DETECTED~~ AEROSOL CHARACTERISTICS AND OCEANIC DIMETHYLSULFIDE
Between Derived

12 PERSONAL AUTHOR(S)
Shema, Richard A.

13a TYPE OF REPORT Master's Thesis	13b TIME COVERED FROM _____ TO _____	14 DATE OF REPORT (Year, Month, Day) 1988, December	15 PAGE COUNT 58

16 SUPPLEMENTARY NOTATION The views expressed in this thesis are those of the author and do not reflect the official policy or position of the Department of Defense or the U.S. Government.

17 COSATI CODES		
FIELD	GROUP	SUB-GROUP

18 SUBJECT TERMS (Continue on reverse if necessary and identify by block number)
Atmospheric aerosol particles — Albedo
Dimethylsulfide — Climate

19 ABSTRACT (Continue on reverse if necessary and identify by block number)

Oceanic dimethylsulfide (DMS), excreted by phytoplankton in the remote ocean, may be a major source of cloud condensation nuclei (CCN). The process includes the formation of non-sea-salt sulfates ($NSS\text{-}SO_4^{-2}$) which serve as a substrate for CCN. The Earth's mean temperature is sensitive to cloud albedo which is a direct function CCN concentration. Therefore, regulation of global climate is possible through variations in oceanic DMS. Two NOAA-7 AVHRR data sets are compared with oceanic DMS measurements. Using two images covering the time periods 20-25 April and 9-12 May 1982, red (Channel 1) and near-infrared (Channel 2) ratios are produced using averaging algorithms. Channel 1/Channel 2 ratio values from these images are compared with oceanic DMS measurements observed from the R/V DISCOVERER between 8-21 May 1982 in the central, equatorial North Pacific Ocean. From this comparison, evidence is presented which supports the relation that oceanic DMS is positively correlated with atmospheric aerosol particles. A slight positive correlation with sea surface temperature and oceanic DMS is also observed.

20 DISTRIBUTION/AVAILABILITY OF ABSTRACT ☒ UNCLASSIFIED/UNLIMITED ☐ SAME AS RPT ☐ DTIC USERS	21 ABSTRACT SECURITY CLASSIFICATION UNCLASSIFIED
22a NAME OF RESPONSIBLE INDIVIDUAL P.A. Durkee	22b TELEPHONE (Include Area Code) (408) 646-3465 — 22c OFFICE SYMBOL Code 63De

DD Form 1473, JUN 86 — Previous editions are obsolete — SECURITY CLASSIFICATION OF THIS PAGE

S/N 0102-LF-014-6603

Approved for public release; distribution is unlimited.

Correlation of Satellite-Detected Aerosol Characteristics
and
Oceanic Dimethylsulfide (DMS)

by

Richard A. Shema
Lieutenant Commander, United States Navy
B.S., Pennsylvannia State University, 1978

Submitted in partial fulfillment of the
requirements for the degree of

MASTER OF SCIENCE IN METEOROLOGY AND OCEANOGRAPHY

from the

NAVAL POSTGRADUATE SCHOOL
December 1988

Author: _____
Richard A. Shema

Approved by: _____
Philip A. Durkee, Thesis Advisor

_____
Carlyle H. Wash, Second Reader

_____
Robert J. Renard, Chairman,
Department of Meteorology

_____
Gordon E. Schacher,
Dean of Science and Engineering

ABSTRACT

Oceanic dimethylsulfide (DMS), excreted by phytoplankton in the remote ocean, may be a major source of cloud condensation nuclei (CCN). The process includes the formation of non-sea-salt sulfates ($NSS\text{-}SO_4^{-2}$) which serve as a substrate for CCN. The Earth's mean temperature is sensitive to cloud albedo which is a direct function CCN concentration. Therefore, regulation of global climate is possible through variations in oceanic DMS. Two NOAA-7 AVHRR data sets are compared with oceanic DMS measurements. Using two images covering the time periods 20-25 April and 9-12 May 1982, red (Channel 1) and near-infrared (Channel 2) ratios are produced using averaging algorithms. Channel 1/Channel 2 ratio values from these images are compared with oceanic DMS measurements observed from the R/V DISCOVERER between 8-21 May 1982 in the central, equatorial North Pacific Ocean. From this comparison, evidence is presented which supports the relation that oceanic DMS is positively correlated with atmospheric aerosol particles. A slight positive correlation with sea surface temperature and oceanic DMS is also observed.

The title on the front cover is correct for this report.
Per Ms. Irna Valantin, NPS/Code 147

TABLE OF CONTENTS

LIST OF TABLES

LIST OF FIGURES

ACKNOWLEDGEMENTS

The research presented here was made possible by the sustained support of several individuals. First, I would like to express my sincere gratitude to Dr. Philip A. Durkee of the Naval Postgraduate School. His thoughtful guidance and unending patience were instrumental in completing the work in a meaningful fashion. Special thanks to Dr. Carlyle H. Wash, also from the Naval Postgraduate School, for his careful review of the manuscript. Dr. Timothy S. Bates, from the Pacific Marine Environmental Laboratory, Seattle, Washington is thanked for providing the shipboard measurements. A special note of thanks to Miss Jeannie Bennett for her technical typing expertise and unyielding patience in processing the manuscript. Finally, a special note of appreciation to Miss Tamlyn Johnson. Her moral support and selfless devotion made possible the completion of this thesis.

I. INTRODUCTION

Since the turn of the century, the earth's climate has fluctuated between warming and cooling cycles. A warming cycle has been observed in the early 1900's. The rising global temperature has been attributed to CO_2 release from the burning of fossil fuels. The trend appears irreversible as the industrialized northern hemisphere continues its dependence on fossil fuels. The dominant optical property of CO_2 is it's strong absorption properties in the infrared (IR) wavelengths. Absorbing material warms the surrounding medium. The absorption of IR energy emitted from the earth, or "greenhouse effect", brought concern that continued warming would melt polar ice caps and permanently change global climate. However, beginning in the mid-1940's, atmospheric cooling was observed. A possible contribution to the cooling trend is an increase in the numbers of relatively small aerosol particles. These particles are efficient scatters of solar radiation. An increase in the number of scattering events causes a higher albedo, thereby creating a cooler planet. McCormick and Ludwig (1967) have presented arguments to show this relationship. Approximately forty years later, in the early 1980's, warming of the earth's climate again has been observed. Atmospheric temperature fluctuation indicate that many processes are operating to produce the observed mean annual temperature.

One such process describes the effect aerosols have on global scale temperature variations. This is hypothesized by Charlson et al.

(1987). He defines a planetary feedback mechanism involving oceanic dimethylsulfide (DMS), atmospheric aerosol particles and cloud-condensation nuclei (CCN). The mechanism is shown in Fig. 1.1. The formation of CCN is the end result of a series of complex biological, chemical and physical processes which transforms waterborne DMS into aerosol particles. In the remote ocean, this sulfur based compound is the major producer of these aerosol particles. DMS is excreted by living algae found throughout the planet's aquatic environment. After ventilation to the atmosphere, DMS is in a highly reactive form and can only exist for a short period of time. Due to it's chemical volatility, it is oxidized within a time scale on the order of a day. The oxidation reaction produces sulfate and methane sulfonate (MSA). The sulfate molecule is the main product and is quickly converted to a non-sea-salt particle ($NSS\text{-}SO_4^{-2}$), because it's chemical composition excludes any one of the halogen elements found in the ocean. These hygroscopic particles are abundant in the marine boundary layer and are smaller in radius than sea-salt particles. Total populations of particles capable of acting as CCN range in size from 30 to 200 cm^{-2}. In the remote ocean, sea-salt particle concentrations are not usually greater than 1 cm^{-3} (Pruppacher and Klett, 1978). Further, the numbers of submicron particles are usually around 200 cm^{-3}. Atmospheric DMS is the most volatile of the atmospheric sulfur components and produces the submicron $NSS\text{-}SO_4^{-2}$ particle. Therefore, Charlson et al. (1987) concludes that the majority of the CCN found in the remote ocean are these same $NSS\text{-}SO_4^{-2}$.

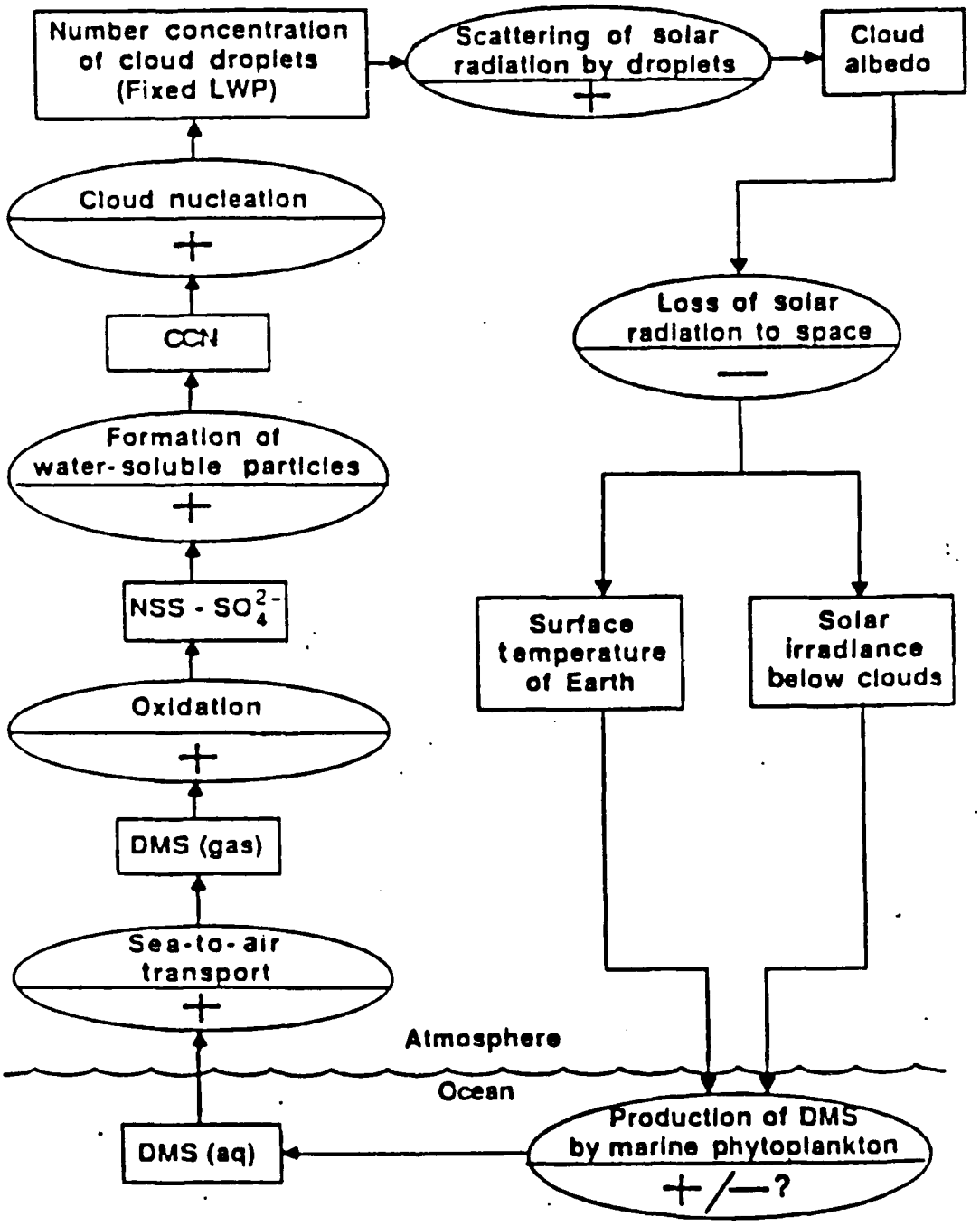

Fig. 1.1 Flow diagram outlining a possible bio-feedback loop regulating climate, from Charlson et al. (1987).

Cloud droplets can only form when there are nuclei present in the atmosphere to serve as a substrate for condensation. A change in distribution of cloud droplets is expected as the concentration of CCN changes (Hobbs, 1974). The result is a change in cloud albedo or cloud reflectance (Twomey, 1977). The earth's temperature is sensitive to changes in cloud albedo because the change in solar radiation available for absorption at the earth's surface is altered Hence, climatic regulation is inferred through a biofeedback process involving organically produced oceanic DMS. (Fig. 1.1).

The use of multispectral satellite sensors has provided the capability to detect the effects of these aerosol particles on backscattered radiance. More exactly, significant variations in aerosol size distributions within the marine boundary layer can be detected. This is due, in part, to the relationship between aerosol particle size and scattered radiance (Durkee, 1984). Knowing the spatial variability of aerosol particles over the remote ocean may provide information about the DMS flux into the atmosphere. An increase in the smaller sized aerosol particles would indicate a greater mass of oceanic DMS transported into the atmosphere. A decrease in aerosol particles reflects a reduced DMS mass transport across the air-ocean interface.

Modeling of global climatology requires an understanding of the effects of aerosol particles on the earth's radiation budget. However, the complex nature of aerosol interaction with clouds and electromagnetic radiation makes it difficult to solve completely the radiative transfer problem. The research presented here will show a

correlation between satellite detected radiance due to aerosol particles and oceanic DMS.

A. BACKGROUND

Electromagnetic energy propagation is a function of atmospheric composition and wavelength of the energy. Of these physical effects, atmospheric composition, including the aerosol particle size distribution, governs optical depth. Griggs (1975) showed that aerosol optical depth is nearly linearly related to aerosol particle size distribution. Therefore, changes in atmospheric particles are manifested by a relative change in upwelled radiance detected at the satellite based sensor (Durkee, 1984).

Aerosol particle sizes responsible for most scattering events at red-visible and near-infrared wavelengths include radii from 0.1 to 10.0 μm (Durkee, 1984). The Advanced Very High Resolution Radiometer (AVHRR) onboard the NOAA-7 satellite, can detect radiances in five channels. Two of the five channels, namely channel 1, red-visible (0.63 μm) and channel 2, near-infrared (0.86 μm), have been used to analyze aerosol and cloud characteristics (Durkee, 1984; Durkee et. al., 1986; Bulfinch, 1986; Pfeil, 1986). Ch1 and Ch2 will be used here to determine if a correlation can be made between upwelled radiance and oceanic DMS concentrations. In an atmospheric experiment conducted in 1982, Durkee et al., (1986) derived a relationship between AVHRR Ch1 and Ch2 radiance with aerosol size distribution as suggested by Griggs (1983). This relationship revealed the satellite detected radiance at Ch1 and Ch2 is positively correlated with aerosol optical depth. Also, the variations of Ch1 to Ch2 ratio (Ch1/Ch2)

indicate variation of the aerosol particle size distribution. An increase in the ratio indicates an increase in small particles relative to large particles. Applying the Ch1/Ch2 ratio relationship to the atmosphere over the remote ocean, regions which have elevated numbers of small atmospheric aerosol particles, such as NSS-SO_4^{-2}, can be determined.

B. OBJECTIVES/MOTIVATION

This study provides supporting evidence that oceanic DMS is positively correlated to atmospheric aerosols. Concentrations of DMS measured in the surface waters of the central, equatorial Pacific Ocean are compared to aerosol characteristics derived from AVHRR detected radiance. Shipboard data were collected from 8 to 21 May 1982 and compared with two sets of AVHRR data from 20-25 April 1982 and 9-12 May 1982. Sampling methods and observations of oceanic DMS are discussed by Cline and Bates (1983). The satellite data are processed using two different but similar climatological algorithms. These algorithms yield images of Ch1/Ch2 ratio values. A direct comparison is then made with surface DMS values. The April data were processed using a procedure described by Pfeil (1986). The May data are processed using Pfeil (1986) as modified by Frost (1988). This procedure eliminated the effects of Rayleigh scattering and absorption due to ozone. These two atmospheric effects combine to increase or decrease the upwelling radiance detected at the sensor. Eliminating them from the processing yields radiance values which reflect only the optical properties resulting from the presence of aerosol particles.

Charlson et al. (1987) reasonably hypothesizes that DMS flux is directly related to the concentration of NSS-$SO4_4^{-2}$ aerosol particles. Therefore, variables that influence the flux should also regulate the aerosol particle distribution observed in the atmosphere.

One final objective is to compare sea-surface temperature (SST) with oceanic DMS because it may be a contributing variable to the atmospheric ventilation process. Several complicated processes make this correlation difficult to predict. A positive correlation would indicate that warmer water is releasing more DMS from the planktonic algae producing the molecule. A negative correlation could be explained by cold, upwelled, equatorial water bringing nutrients into the photic zone so that primary production can occur. More DMS would be produced with an increase in photosynthetic activity, provided that DMS producers were present. Currently, not enough information is known about the chemistry of DMS, or the algae that produce it, to completely explain the intricate mechanisms occurring in the ocean.

This thesis is composed of five chapters. Chapter II describes the theory of radiative transfer and the simplifying assumptions and approximations required for single scattering in the remote marine boundary layer. Analysis of the shipboard data and a description of the two climatological algorithms producing Ch1/Ch2 ratio values from the satellite data are presented in Chapter III. In Chapter IV, a comparison is made between the shipboard data and the Ch1/Ch2 ratio images and correlations are made between the two. Conclusions and recommendations for future research are the subject of the final chapter.

II. THEORY OF RADIATIVE TRANSFER

As electromagnetic energy passes through the atmosphere, it's propagation is affected in several ways. Through attenuation, radiation is absorbed and scattered by atmospheric constituents. The composition of the atmosphere and wavelength of the energy determines the extent of absorption and scattering by the medium. Within the marine boundary layer over the remote ocean, the composition of the atmospheric aerosol is composed mostly of submicron sized particles in the form of NSS-SO_4^{-2} and some supermicron sized particles. This bimodal distribution is shown in Fig. 2.1 (Clarke et al., 1987).

This observation allows us to make several assumptions and approximations to simplify the radiative transfer equation (RTE). Measuring the upwelled radiance using satellite sensors, we can estimate the aerosol particle characteristics of the marine atmosphere. Scattering of radiation depends on the size and shape of the particles interacting with the radiation. Rayleigh or molecule scattering occurs when particles interact with electromagnetic energy of much longer wavelength ($r \ll \lambda$). Particle size on the same order of magnitude as the wavelength results in Mie scattering. When particle size significantly exceeds the wavelength ($r \gg \lambda$), scattering is geometric.

Absorption of incident radiation, like scattering, is wavelength and composition dependent. Gases composing the earth's atmosphere are strong absorbers at wavelengths outside the visible spectrum (0.4 to

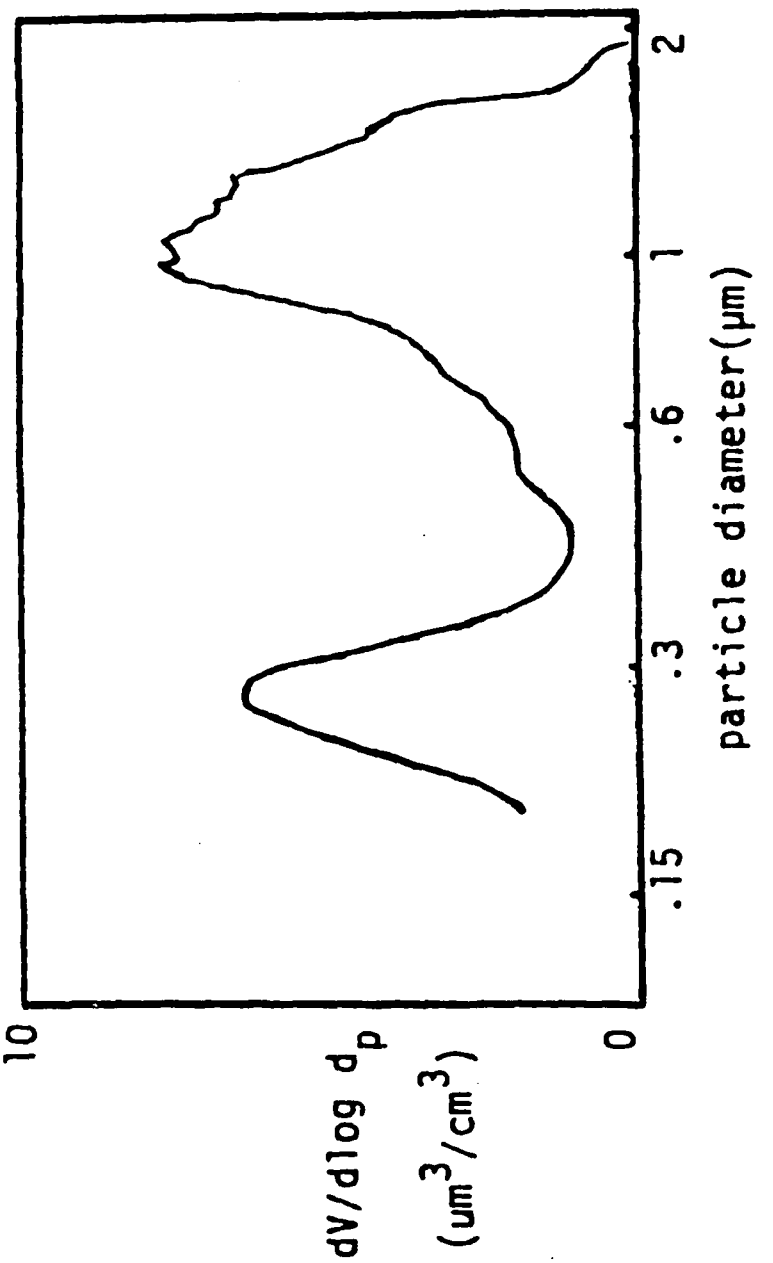

Fig. 2.1 Volume distribution of atmospheric aerosol particles versus particle diameter, from Clarke et al. (1987).

0.7 um). Fig. 2.2 shows the absorption spectrum of the atmosphere (Fleagle and Businger, 1980). Satellite sensors, such as the Advanced Very High Resolution Radiometer (AVHRR) aboard the polar orbiter NOAA 7, measures the upwelled radiance at wavelengths where atmospheric absorption is minimal. Among these regions, red-visible (Ch1) and near infrared (Ch2) are important in the study of aerosols. These channels measure upwelled radiance in bandwidths around the weighted mean wavelengths of 0.63 μm and 0.86 μm respectively. Fig. 2.3 shows the spectral response of channels 1 and 2 of the NOAA 7 AVHRR sensor (Gruber et al., 1983). Since the aerosol particle radii within the marine boundary layer are of the same order of magnitude as the detected wavelength of these channels, Mie theory will explain the scattered energy measured at the sensor. Spatial or temporal variability in upwelled radiance reflects a change in size, number and composition of aerosol particles.

Atmospheric interference with propagating electromagnetic radiation is represented quantitatively by the radiative transfer equation. We assume the top and bottom of the atmosphere are plane parallel. This is required to simplify the radiative transfer calculations and is justified because incoming and upwelled beams are almost perpendicular to the atmosphere. Liou (1980) describes the complete equation as

$$\frac{\mu dL(\delta,\Omega)}{d\delta} = L(\delta,\Omega) - \frac{\omega_o}{4\pi}\int_{4\pi} L(\delta,\Omega')\, P(\Omega,\Omega')\, d\Omega' \qquad (2.1)$$

$$- \frac{\omega_o \pi}{4\pi} F_o P(\Omega,-\Omega_o)\, e^{-\delta(1/\mu + 1/\mu_o)},$$

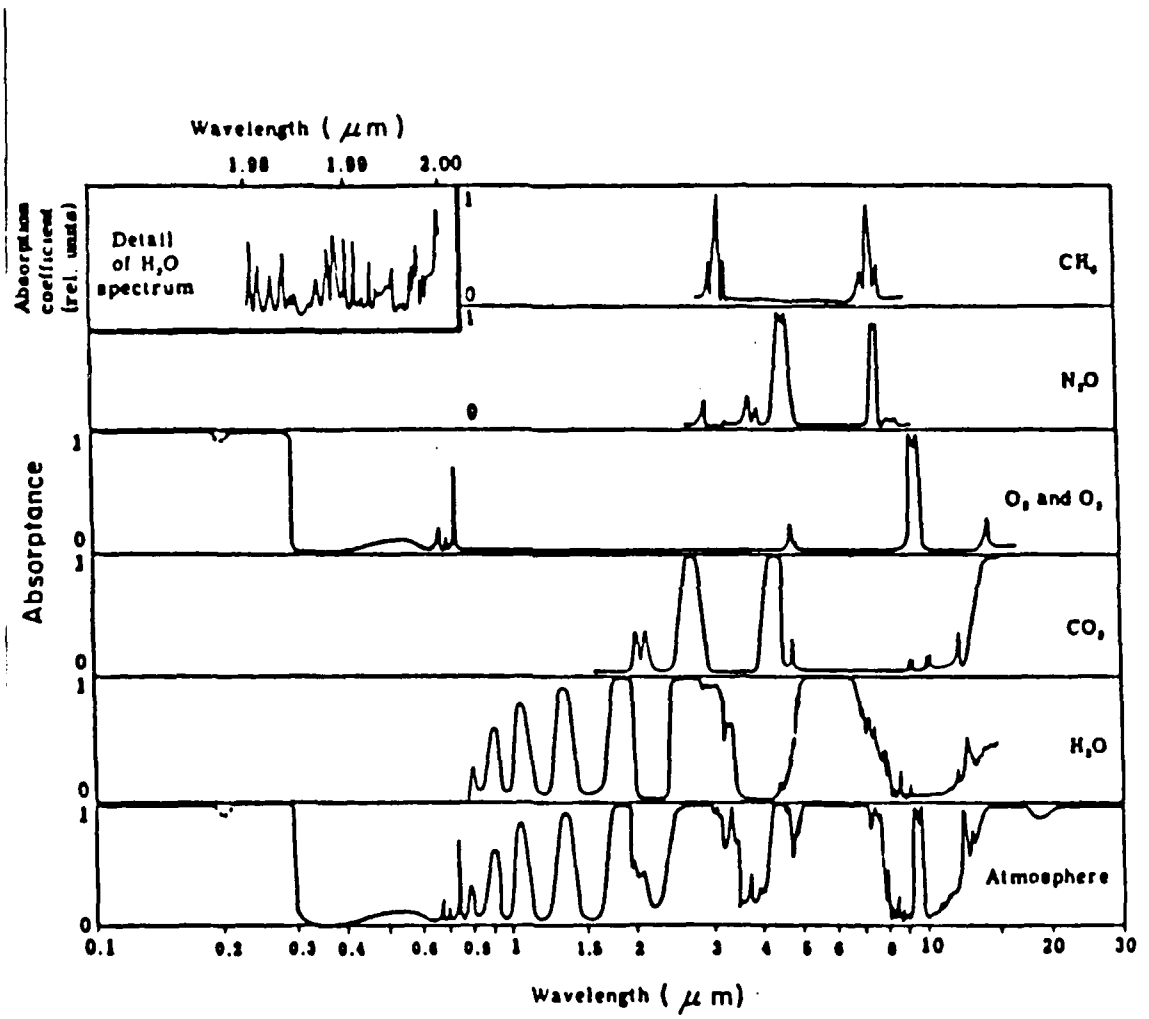

Fig. 2.2 Absorptance spectrum for the earth's atmospheric gases, from Fleagle and Businger (1980).

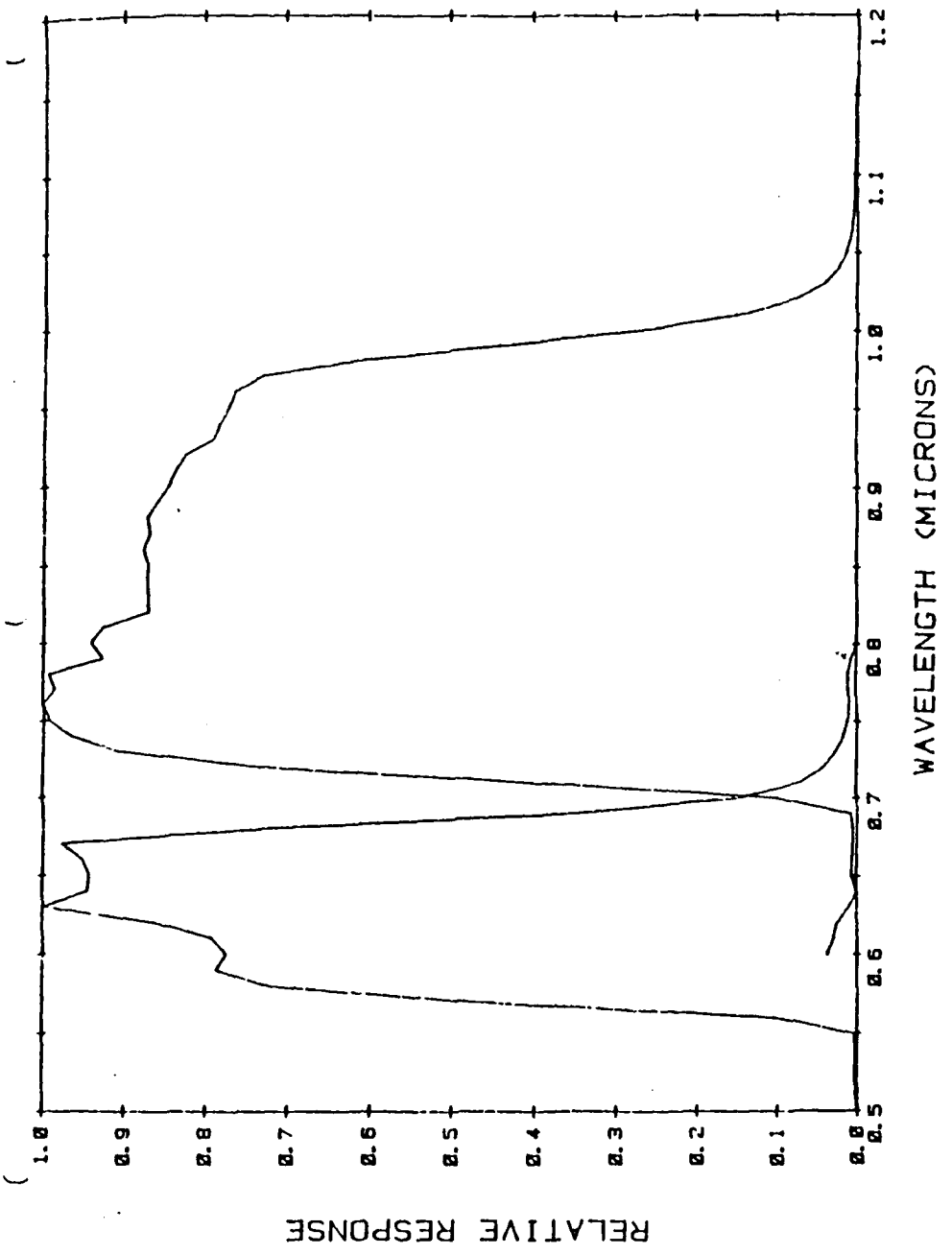

Fig. 2.3 Spectral response of the AVHRR channels 1 (0.63μm) and 2 (0.86 μm), from Gruber et al. (1983).

where

L = diffuse intensity of radiance,

δ = optical depth,

ω_o= single scattering albedo,

μ = cos θ; where θ is the satellite zenith angle,

μ_o= cos θ_o; where θ_o is the solar zenith angle,

Ω = angular direction of upwelled beam (θ, ϕ),

$P(\Omega,\Omega')$ = scattering phase function and

πF_o= incoming solar radiative flux.

The terms on the right hand side explain the intensity lost due to attenuation, the intensity gained by multiple scattering into the beam from all directions and the beam addition term accounting for single scattering events. The physical orientation of the sun-earth-satellite system also affects the amount of upwelled radiation reaching the sensor. This angular dependence is described by solar angles and sensor viewing angles. The angles, θ_o, and solar azimuth (ϕ_o) represent the direction of the solar beam, Ω_o. The view direction of the satellite is described by (θ, ϕ) or Ω. Fig. 2.4 depicts the viewing geometry (Liou, 1980).

To solve equation 2.1, information regarding the optical properties of the marine layer is required. This allows inputs to the RTE concerning optical depth, scattering phase function and single scattering albedo. The measured radiance at the sensor then reveals the nature of atmospheric aerosol particles that is scattering the energy.

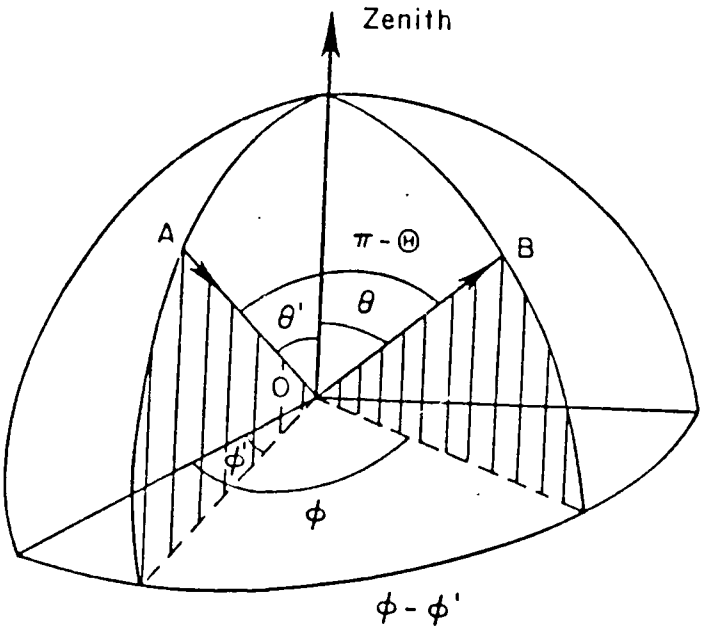

Fig. 2.4 Relation of scattering, zenith and azimuthal angles, from Liou (1980).

The coefficients that describe extinction and scattering are defined from (Bohren and Huffman, 1983) as

$$\beta_{ext} = \int_0^\infty \pi r^2 \, Q_{ext}(m,r) \, \frac{d\,N(r)}{dr} dr, \tag{2.2}$$

$$\beta_{scat} = \int_0^\infty \pi r^2 \, Q_{scat}(m,r) \, \frac{d\,N(r)}{dr} dr \tag{2.3}$$

and

$$\beta_{abs} = \int_0^\infty \pi r^2 \, Q_{abs}(m,r) \, \frac{d\,N(r)}{dr} dr, \tag{2.4}$$

where

r	= particle radius,
Q_{ext}	= extinction efficiency,
Qscat	= scattering efficiency,
Q_{abs}	= absorption efficiency,
m	= complex index of refraction and
dN(r)/dr	= the particle size distribution.

Extinction is the sum of absorption and scattering effects and is represented by

$$\beta_{ext} = \beta_{abs} + \beta_{scat}. \tag{2.5}$$

From equations 2.2 and 2.3, the extinction and scattering coefficients are the integration over radius of the product of the cross sectional area of aerosol particles, the extinction or scattering efficiency and the size distribution. Fig. 2.5 a, b and c presents these relations with particle radius at 80% relative humidity (Shettle and Fenn, 1979). At small particle radius, the cross sectional area (πr^2) is small as is the extinction efficiency due to scattering (Q_{scat}).

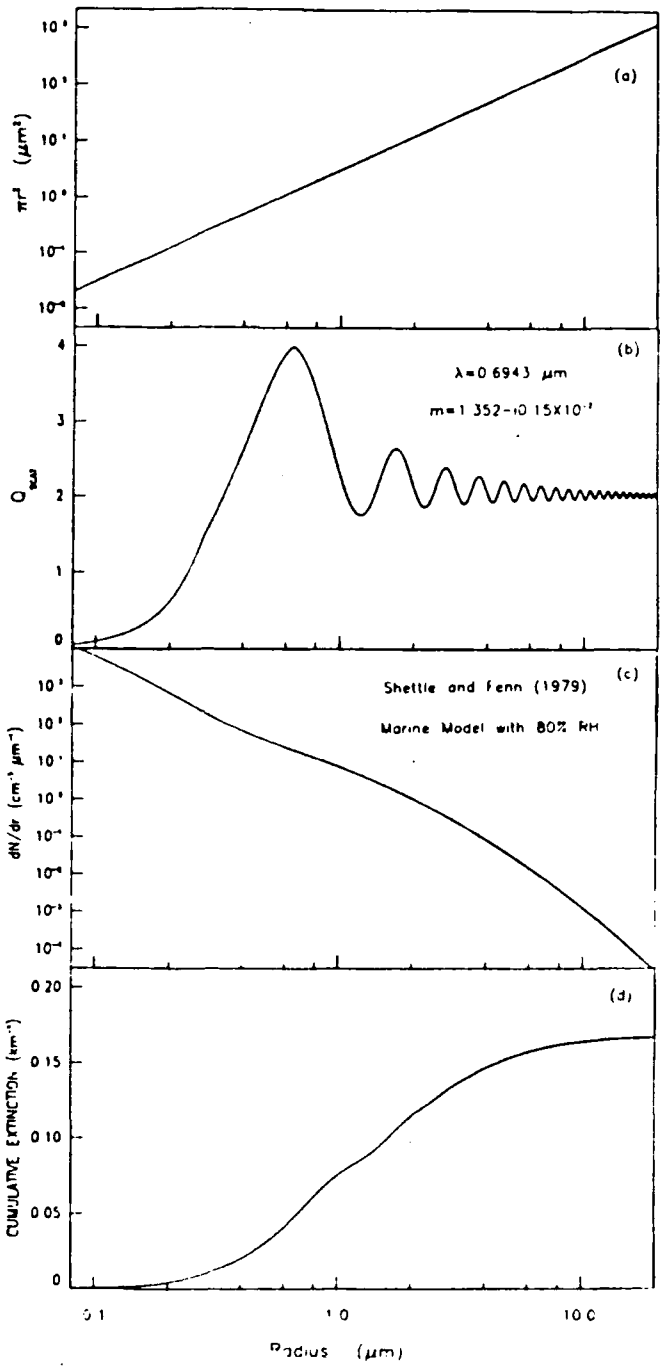

Fig. 2.5 The terms of Equation 2.2 as a function of radius: (a) πr^2, cross sectional area; (b) Qscat, scattering efficiency; (c) dn/dr, the particle size distribution; (d) cumulative extinction.

However, the size distribution (dN/dr) shows a large number of small radius particles. The cross sectional area of large radius particles is understandably large and the Q_{scat} approaches an asymptotic value of two. Contrarily, dN/dr becomes small at large radii. These effects combine to produce a cumulative extinction depicted in Fig. 2.5d. The area of significant slope bounds the radii that contributes most to β_{ext}. For a marine environment with 80% relative humidity and a visible wavelength of 0.6943 μm, this region is 0.1 μm to 10.0 μm (Durkee, 1984).

The optical depth is defined as the vertical integration from the surface to the satellite altitude H of the extinction coefficients:

$$\delta = \int_0^H \beta_{ext}\, dz. \tag{2.6}$$

The single scattering albedo now can be introduced. Absorption by aerosol particles are highly wavelength dependent but the effect is very small for $\lambda < 1$ μm (Shettle and Fenn, 1979). This means that absorption is small at the wavelengths of interest (AVHRR Ch1 and Ch2) and $\beta_{ext} \sim \beta_{scat}$. The ratio of β_{scat} to β_{ext} indicates the efficiency of the scattering medium and is called the single scattering albedo. It is defined as

$$\omega_o = \frac{\beta_{scat}}{\beta_{ext}}. \tag{2.7}$$

Since aerosol particles are efficient scatterers, the ratio approximates one.

The scattering phase function $P(\Omega,\Omega_o)$ describes the angular distribution of the scattered radiation. The phase function varies greatly with particle sizes. For the marine environment, Mie theory can be used to calculate $P(\Omega,\Omega_o)$. This is because particles are mostly submicron in size and spherical in shape due to their hygroscopic nature. The scattering phase function for a modeled marine particle distribution at 80% relative humidity is plotted in Fig. 2.6 (Shettle and Fenn, 1979). Most scattering events occur in the forward direction, with very little backward or side scattering.

Examination of equation 2.1 reveals several simplifications. The multi-scattering term can be neglected because the marine environment can be characterized by a small optical depth. Over the remote ocean, optical depth measurements are usually less than 0.1. Globally, optical depth varies between 0.003 to 3.000 (World Climate Research Programme, 1986). The probability of a scattering event occurring with the same photon more than once is small. Therefore, the multiple interaction term can be neglected and a single scattering approximation is made. The albedo of the ocean is less than 0.5% at red wavelengths and almost zero for wavelengths greater than 0.7 μm. Since we are concerned with wavelengths in this range, we can assume reflectance from the ocean is nearly zero (Ramsey, 1968). Considering the simplifications discussed, equation 2.1 reduces to

$$L(0;\mu,\phi) = \frac{\omega_o \mu_o F_o}{4(\mu+\mu_o)} P(\Theta) \left[1 - e^{-\delta(1/\mu + 1/\mu_o)}\right], \qquad (2.8)$$

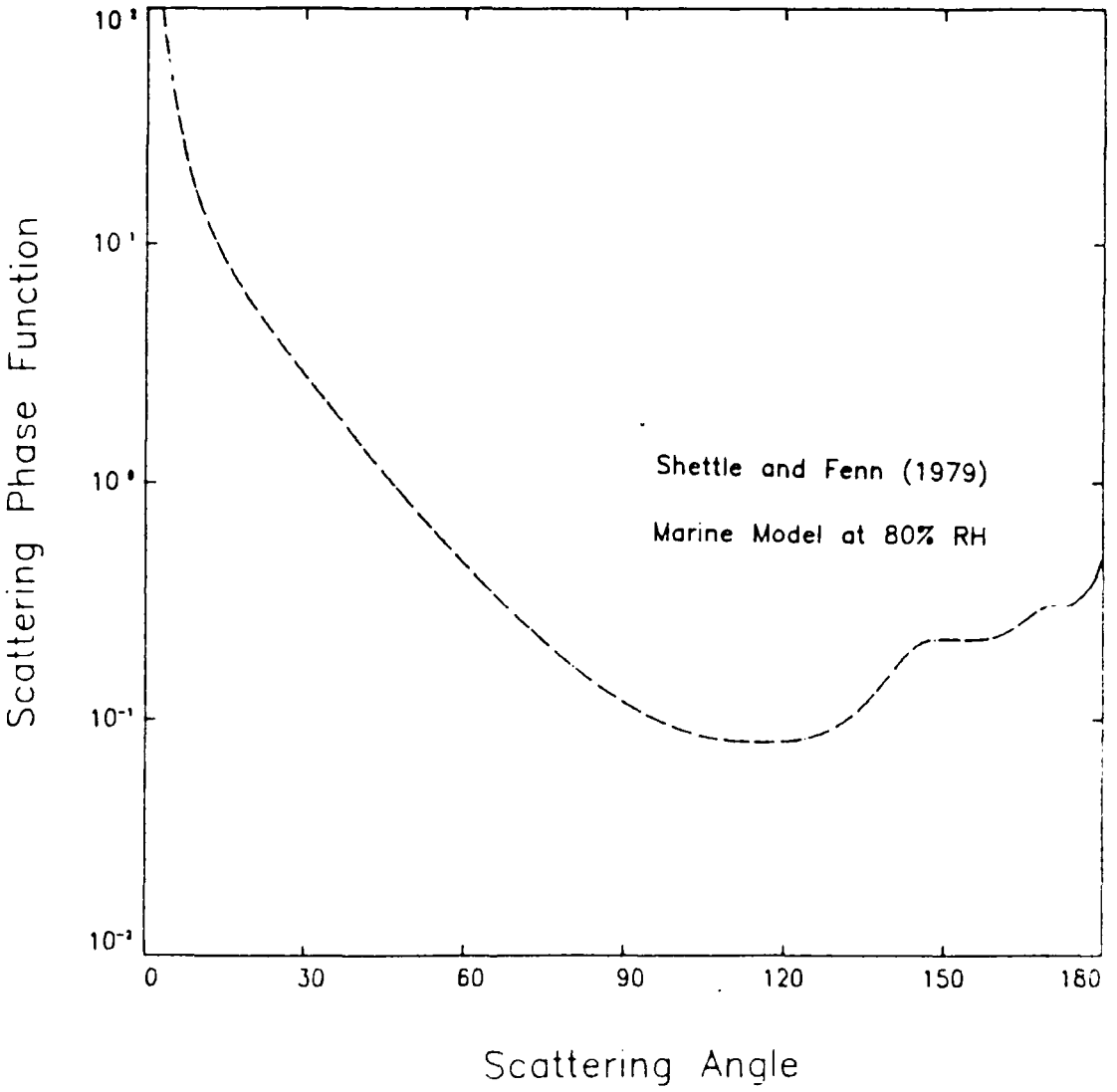

Fig. 2.6 The single scattering phase function for the model of the marine particles at 80% relative humidity, from Shettle and Fenn (1979).

where Θ is the single scattering angle. For a small value of optical depth, and solar and satellite zenith angles, the term $\delta(1/\mu + 1/\mu o)$ is also small and the RTE now becomes:

$$L(0;\ \mu,\phi) \sim (\frac{\omega_o F_o}{4\mu})\ P(\Theta)\delta. \tag{2.9}$$

The scattering phase function does not vary appreciably with wavelength. Our objective is to detect variations of aerosol particle size distribution over an ocean region. Noting the upwelled radiance at different wavelengths, Durkee (1986) determined that aerosol dependent terms in equation 2.1 are of larger value at red wavelengths than at near infrared wavelengths. Observing the difference in upwelled radiance at these two wavelengths reveals information on aerosol particle sizes. We can develop a ratio using equation 2.9 for red and near infrared wavelengths to measure this difference,

$$\frac{L_{red}}{L_{nir}} \sim \frac{[(\frac{\omega_o F_o}{4\mu})\ P(\Theta)\delta]_{red}}{[(\frac{\omega_o F_o}{4\mu})\ P(\Theta)\delta]_{nir}}. \tag{2.10}$$

For smaller particles, such as those produced by DMS emissions, the numerator will be larger giving a larger value for the ratio. For ocean regions of lower DMS concentrations, we would expect a reduction in the ratio due to fewer small particles.

The total diffuse radiance, L, is the summation of radiance due to aerosol scattering, L_A, and Rayleigh scattering, L_R. It was shown by Pfeil (1986) that L_R can be a large term in L, but has little spatial

variability. This is especially true over the equatorial regions where satellite viewing geometry does not change appreciably. To strictly observe the change in radiance due only to aerosol particle distribution, the effect of Rayleigh scattering is removed. The ratio is now expressed as

$$\frac{L_{red} / F_0}{L_{nir} / F_0} \sim \frac{(\delta_A)_{red}}{(\delta_A)_{nir}}, \qquad (2.11)$$

where δ_A is aerosol optical depth. Equation 2.11 describes the relationship between diffuse radiance and aerosol optical depth in two wavelengths. The radiance values at red-visible (Ch1) and near-infrared (Ch2) can be measured by satellite sensors. Therefore, variations of aerosol particle size in the remote marine atmosphere can be resolved. Environmental satellites provide global coverage and can supply the data necessary to compute Ch1/Ch2 ratio. Spatial variability of the ratio, especially over the remote oceans, can be determined. As will be shown, the Ch1/Ch2 ratio is a valuable tool to help understand aerosol particle distribution.

III. DATA ANALYSIS

To determine the correlation between DMS and variations in aerosol particle size, shipboard measurements of DMS were compared with satellite detected Ch1/Ch2 ratio values. The shipboard data were obtained from the R/V DISCOVERER, a National Oceanic Atmospheric Administration (NOAA) funded research vessel. The data were received from the Pacific Marine Environmental Laboratory (PMEL) at Seattle, Washington. Data sampling began on 8 May 1982 and was completed on 21 May 1982 (Cline and Bates, 1983). From the beginning sampling location at 17.7°N, 156.2°W, the ship traveled south - southeast arriving at the equator at 148.0°W. The vessel then headed due west along the equator to 170.0°E then turned due north to 5°N and completed the sample collection at 6.9°N and 168.5°E just south of the Marshall Islands. The ship track is depicted in Fig. 3.1. Channel 1 and 2 radiance values were produced from data samples observed from NOAA-7. The image data were collected by the Advanced Very High Resolution Radiometer (AVHRR) sensor onboard the satellite. NOAA-7 is a TIROS-N series sun synchronous, polar orbiting satellite with a period of 102 minutes and an ascending node at 1430 and a descending node at 0730. (All times local). An instantaneous field of view of about 1.4 milliradians and a nominal altitude of 833 km provides a suborbit resolution of approximately 1.1 km.

The AVHRR samples data at five channels ranging from visible to infrared wavelengths. Channels 1 and 2 with bandwidths of 0.58 to

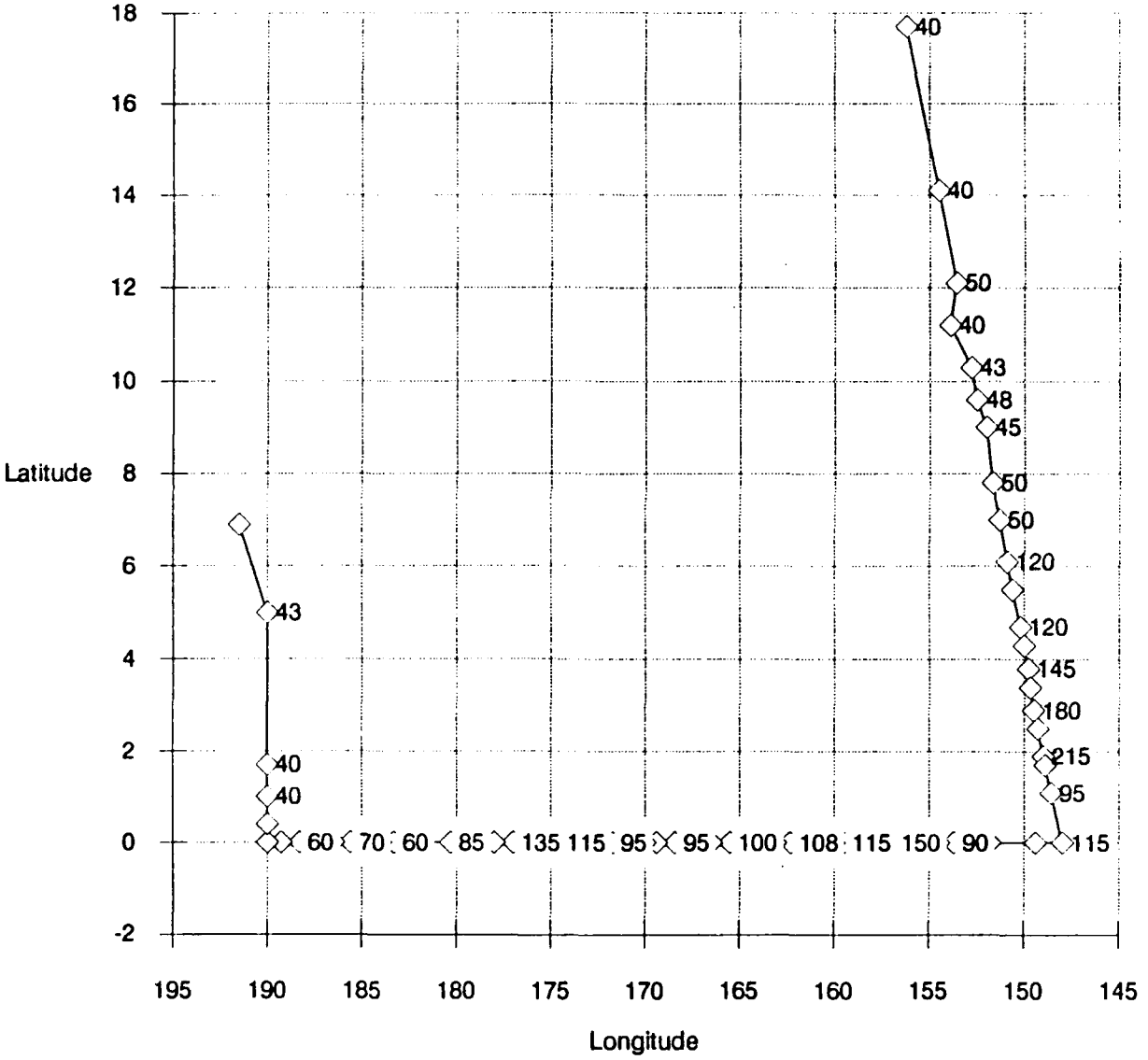

Fig. 3.1 8-21 May 1982 shiptrack of the R/V DISCOVERER with selected values of surface DMS (ng/l).

0.68 μm and 0.725 to 1.1 μm, respectively, were used here. The spectral response of channels 1 and 2 were shown earlier in Fig. 2.3.

The radiation sampling procedures consists of an instrument scan rate of six scans per second perpendicular to the orbital path. A local area coverage (LAC) spot or picture element (pixel) is formed using 2048 samples. For processing large areas, LAC data are reduced further to form global area coverage (GAC) data. This minimizes archiving requirements. Reduction of LAC data is completed onboard the satellite by averaging four of every five continuous LAC spots per scan line. The succeeding two scan lines are omitted with the averaging procedure continuing then on the fourth line. The resulting suborbit resolution for GAC data are approximately 3.3 km by 4.0 km.

Two data sets were available for comparison with shipboard measurements. The first data set, 20-25 April 1982, was obtained from Pfeil (1986). The second set, 9-12 May 1982, coincided with the shipboard measurements. This data set was received upon request from the National Environmental Satellite Data and Information Service (NESDIS). Processing the data produced images in Ch1/Ch2 ratio values that were then compared with the shipboard measurements of DMS.

The April data were processed by Pfeil (1986) using an averaging algorithm. The algorithm averaged GAC data within a one degree latitude by one degree longitude box. The data were checked for the presence of clouds and sunglint by using Ch1/Ch2 albedo ratio, Ch4 (11.0 μm) temperatures and visual inspection of AVHRR imagery. A pixel with an albedo ratio less than a threshold of 1.3 was considered to be contaminated by clouds and eliminated from the data. Ch4

temperature, with a bandwidth of 10.3 - 11.3 μm, was used to detect the presence of high thin cirrus. A pixel with a value greater than 250 counts was defined to be cirrus contaminated. Sunglint was subjectively eliminated by visually examining the images. Most of the sunglint was located on the western edge of the image. Therefore, this area was eliminated. This conservative procedure ensured minimum contamination at the expense of some clear pixels.

The May data were processed using an improved edition of Pfeil (1986) processing methods developed by Frost (1988). This procedure conducted a better check on cloud and sunglint contamination. The algorithm eliminates the effects of two atmospheric radiative phenomena. First, Rayleigh scattering contributes to the satellite detected radiance due to molecular scattering. Second, the presence of ozone in the stratosphere absorbs radiation that would otherwise be available for scattering in the marine boundary layer. These two radiative processes are removed from the radiance values at channels 1 and 2, since only the effects of aerosol particles are desired. The updated version was also developed at the Naval Postgraduate School using the computer facilities in the Meteorology/Oceanography Interactive Digital Environmental Analysis (IDEA) Laboratory.

IV. RESULTS

This chapter describes the relation of the shipboard observations with the satellite data. First, a discussion of the shipboard observations is presented. Second, the April Ch1/Ch2 ratio imagery are compared with the ship measurements. Lastly, a comparison is made between the May data and shipboard measurements during the same week of operations.

The ship began recording environmental data on 8 May 1982 at 17.7° N, 156.2°W, approximately 150 n mi south of Hawaii. The recorded information at each sampling station included ocean surface DMS concentrations, sea-surface temperature, air temperature, wind direction, and speed and observed weather conditions. Sampling sites were not at constant spatial intervals but varied between 230 and 6 n mi with the average being 55 n mi. Fig. 3.1 shows the ship sampling sites with representative DMS concentrations in nanograms per liter (ng/l) observed along the route. Table 1 displays the complete data fields collected by the ship. The ship track is divided into three legs. A discussion of the observed DMS values is described below.

Concentrations of oceanic DMS ranged from 40 to 215 ng DMS/l along the segment extending south of Hawaii. The lower values were contained north of 6.1°N. An approximate three fold increase is observed at the position 6.1°N, 150.9°W and this high level is maintained southward to the equator. The highest sampled value of 215 ng DMS/l is observed at 1.9°N, 149.0°W. The discontinuity at

TABLE 1: SHIPBOARD MEASUREMENTS OF DMS, SST AND SURFACE WINDS FOR MAY 8-21, 1982 AND CH1/CH2 RATIO FOR APRIL 20-25, AND 8-12 MAY, 1982.

Date	Time	DMS ngs/l	Lat °N	Long °W/E	SST log(°C)	Ch1/Ch2 20-25 Apr	Wind KTS	Ch1/Ch2 8-12 May
50882	1800	40	17.7	156.2°W	25.1	1.48	22	1.48
50982	1000	40	14.1	154.5	26.3	0.00	21	1.49
50982	2000	50	12.1	153.6	27.2	0.00	25	1.47
51082	0030	40	11.2	153.9	27.4	1.48	26	1.55
51082	0415	43	10.3	152.8	27.4	0.00	25	0.00
51082	0800	48	9.6	152.5	27.5	1.40	20	1.51
51082	1245	45	9.0	152.0	27.8	0.00	14	0.00
51082	1615	50	7.8	151.7	28.2	1.34	19	1.48
51082	2000	50	7.0	151.3	28.3	1.59	14	1.52
51182	0000	120	6.1	150.9	28.4	1.71	8	1.54
51182	0230	100	5.5	150.6	28.5	1.71	11	1.54
51182	0600	120	4.7	150.2	28.3	1.81	10	1.62
51182	0800	210	4.3	150.0	28.3	1.86	14	1.55
51182	1000	145	3.8	149.8	28.3	1.86	14	1.58
51182	1200	195	3.4	149.7	28.0	1.77	14	1.58
51182	1415	180	2.9	149.5	28.0	1.77	17	1.65
51182	1610	180	2.5	149.3	28.2	1.79	14	1.65
51182	1830	215	1.9	149.0	28.1	1.79	14	1.66
51182	2030	195	1.7	148.9	28.0	1.79	19	1.66
51182	2320	95	1.1	148.6	28.0	1.85	20	1.57
51282	0450	115	0.0	148.0	27.8	1.87	18	1.68
51282	0700	123	0.0	148.0	27.8	1.87	13	1.68
51282	0730	108	0.0	149.4	27.7	1.87	15	1.64
51282	1230	115	0.0	149.4	27.8	1.87	8	1.64
51282	1830	100	0.0	151.8	27.3	1.83	10	1.56
51382	0020	75	0.0	152.3	27.4	1.83	8	1.56
51382	1230	90	0.0	153.7	27.1	1.85	12	1.60
51382	1620	80	0.0	154.5	27.6	1.81	7	1.60
51382	2035	80	0.0	155.6	27.6	1.85	7	1.59
51482	0130	150	0.0	156.9	27.5	1.74	6	1.59
51482	0430	108	0.0	157.1	27.6	1.74	6	1.59
51482	0800	85	0.0	158.4	27.7	1.67	3	1.59
51482	1230	115	0.0	159.5	27.7	1.81	6	1.54
51482	1600	130	0.0	160.0	27.8	1.81	3	1.53
51482	2000	115	0.0	160.8	27.8	1.84	0	1.53
51582	0100	108	0.0	162.3	27.8	1.91	0	1.47
51582	0400	85	0.0	163.1	27.8	1.86	0	1.47
51582	0800	95	0.0	164.1	27.8	1.89	7	1.44
51582	1545	100	0.0	165.5	28.3	1.79	6	1.39
51582	2000	95	0.0	166.5	28.4	1.79	6	1.39
51682	0015	95	0.0	167.5	28.3	1.80	5	1.43
51682	0400	95	0.0	168.4	28.3	1.80	3	1.43
51682	0800	130	0.0	169.4	28.2	1.80	8	1.53
51682	1300	115	0.0	170.0	28.4	1.76	5	1.53

Date	Time	DMS ng/l	Lat °N	Long °W/°E	SST log(°C)	Chl/Ch2 20-25 Apr	Wind kt	Chl/Ch2 8-12 May
51682	0015	95	0.0	167.5°W	28.3	1.80	5	1.43
51682	0400	95	0.0	168.4	28.3	1.80	3	1.43
51682	0800	130	0.0	169.4	28.2	1.80	8	1.48
51682	1300	115	0.0	170.0	28.4	1.76	5	1.53
51682	2000	95	0.0	171.7	28.6	1.81	6	1.53
51782	0000	85	0.0	172.7	28.6	1.77	10	1.55
51782	0400	115	0.0	173.7	28.7	1.78	12	1.53
51782	0800	115	0.0	174.6	28.8	1.79	10	1.56
51782	1200	120	0.0	175.1	28.8	1.79	15	1.56
51782	1600	135	0.0	176.0	29.0	1.78	8	1.48
51782	2000	135	0.0	177.0	29.1	1.69	12	1.48
51882	0000	135	0.0	178.0	29.0	0.00	10	1.49
51882	0800	70	0.0	180.0	29.3	0.00	14	*
51882	1200	85	0.0	179.7°E	29.5	0.00	14	*
51882	1600	78	0.0	179.7	29.9	0.00	11	*
51882	2000	70	0.0	177.8	29.9	0.00	10	*
51882	2400	60	0.0	176.7	29.9	1.80	14	*
51982	0430	65	0.0	175.6	29.9	1.74	17	*
51982	0800	80	0.0	174.0	29.6	1.74	20	*
51982	1200	70	0.0	173.4	29.8	1.83	14	*
51982	1600	60	0.0	173.5	29.9	1.83	11	*
51982	2030	80	0.0	172.5	29.7	1.77	10	*
52082	0000	60	0.0	171.0	29.6	1.77	7	*
52082	0400	38	0.0	170.0	29.5	1.57	5	*
52082	0800	40	0.0	170.0	29.4	1.61	5	*
52082	1200	43	0.4	170.0	29.5	1.61	6	*
52082	1600	40	1.0	170.0	29.5	1.48	0	*
52082	2000	40	1.7	170.0	29.6	1.47	11	*
52182	1230	43	5.0	170.0	29.2	1.37	12	*
52182	2230	43	6.9	168.5	28.8	1.40	10	*

* Indicates satellite data not available for these dates.

approximately 6°N can be explained by the increased primary production in the region of equatorial divergence south of this area. Diverging water produces an upwelling of nutrients into the photic zone from below, thereby increasing phytoplankton abundance.

To the north of 6°N, westward flowing waters of the South Equatorial Current and the eastward flowing waters of the North Equatorial Counter Current provide Ekman convergence. Downwelling of surface waters in the area prevents nutrients from reaching the upper layer. The reduced plankton activity is manifested by the depressed DMS concentrations. Located further north is the subtropical Pacific gyre, known for its reduced primary productivity (Clarke, et al. 1987; Andreae and Raendonck, 1983).

Charlson et al. (1987) showed that primary production activity does not necessarily correlate directly with DMS concentrations. The microbial breakdown of DMS is a nonlinear removal process. Bacteria are able to metabolize DMS in the ocean, making it unavailable for ventilation to the atmosphere. This metabolic removal process is dependent upon the density of bacteria and the concentration of oceanic DMS. The population of bacteria that have the ability to breakdown DMS, and the rate at which metabolism occurs, depends on nonlinear relationships between phytoplankton densities and the grazing organisms. Additionally, not all algae species produce DMS and the ones that do rarely produce the chemical at the same rates. Coccolithophores, for an example, produce DMS at a rate three times faster than most other algae. So, the DMS-primary productivity relation is not necessarily observed. However, in this case, the DMS

gradient appears to be related to the region of expected primary productivity.

Proceeding westward along the equator, the DMS quantities maintain relatively high values above 100 ng DMS/l with some areas of localized minimums. After crossing 180°W, the values decrease by almost a factor of two to about 40 ng DMS/l (Fig. 3.1; Table 1). This minimum value was located at 0°N, 170°E. From 170°E, the ship proceeded due north on its final leg of the cruise. The values observed along this final section maintained the low DMS quantities observed east of the date line. This is in contrast to the values between the equator and 6°N, 150°W.

The DMS values measured by R/V DISCOVERER are in agreement with previous observations in the region. The results of another sampling expedition were reported by Andreae and Raendonck (1983). A meridional leg running 23°N to 4°S at 140°W had values ranging from 50-140 ng DMS/l. An east-west track (80-140°W) along 1°N latitude had values ranging from about 60 ng DMS/l to as high as 315 ng DMS/l. Equatorial waters of the North and South Atlantic ocean had similar concentrations as reported by Barnard et. al. (1982) which was the first extensive study of oceanic DMS. As was seen in the western North Pacific, the western equatorial North Atlantic region displayed lower values with a mean of 60 ng DMS/l. However, the variability of DMS was much greater with observed values between 18 and 743 ng DMS/l. The most variable concentrations were in both North and South Atlantic (Barnard et al., 1982).

The sea-surface temperature values recorded were typical of the equatorial region. At 17.7°N, 156.2°W the temperature was at a minimum of 25.1°C. Temperatures slowly increased southward, attaining a local maximum at 5.5°N, 150.6°W. South of this point, the sea-surface temperatures began to cool, reaching a local minimum of 27.1°C at 0.0°N, 153.7°W. This supports the inference that equatorial upwelling is occurring in the region. The trend then turns upward along the equator, approaching it's highest value of 29.9°C at 0.0°N, 180.3°E. These high values, ranging from 29.9°C to 29.2°C, are maintained throughout the remainder of the sampling period. Observing the relatively low DMS concentrations in the same area of warm water would indicate a local region of downwelling or decreased upwelling. Fig. 4.1 displays representative sea-surface temperatures recorded during the cruise.

Next, we examine the 20-25 April and 9-12 May 1982 AVHRR analysis. The 20-25 April analysis was produced from an algorithm developed by Pfeil (1986). Recall from earlier discussion that this procedure produced an image composed of Ch1/Ch2 ratio values which included Rayleigh scattering and the absorptive properties of ozone. The May results were produced with Frost (1988). The path added radiance due to Rayleigh scattering and the absorption properties of ozone at the wavelengths of interest were eliminated.

The color enhanced Ch1/Ch2 ratio image from the 20-25 April 1982 data set is shown in Fig. 4.2. The shiptrack during the 8-21 May period is outlined in white. A clear observation is the relatively high ratio values located throughout the North and South Pacific

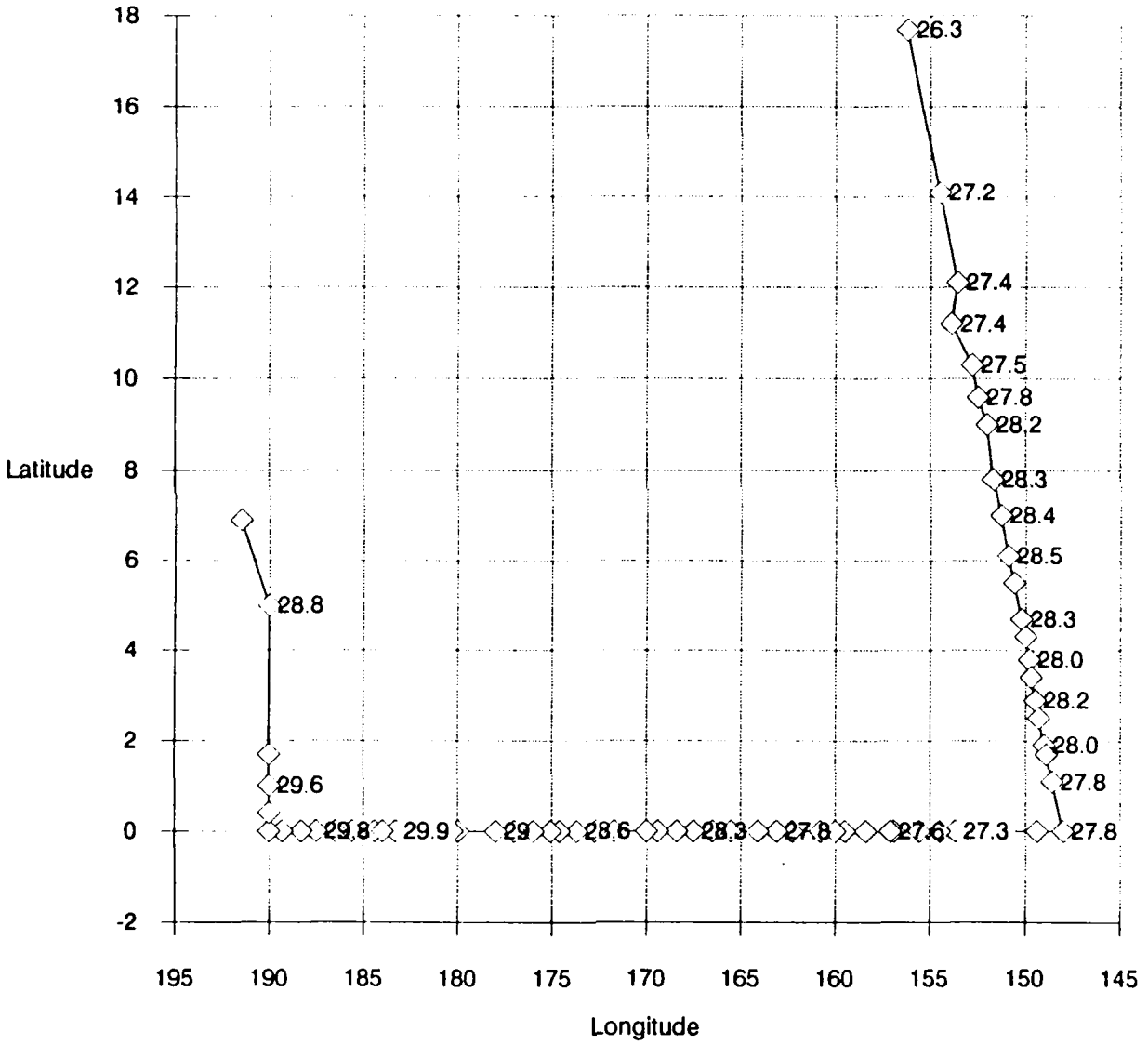

Fig. 4.1 8-12 May 1982 shiptrack of the R/V DISCOVERER with selected values of sea-surface temperature (°C).

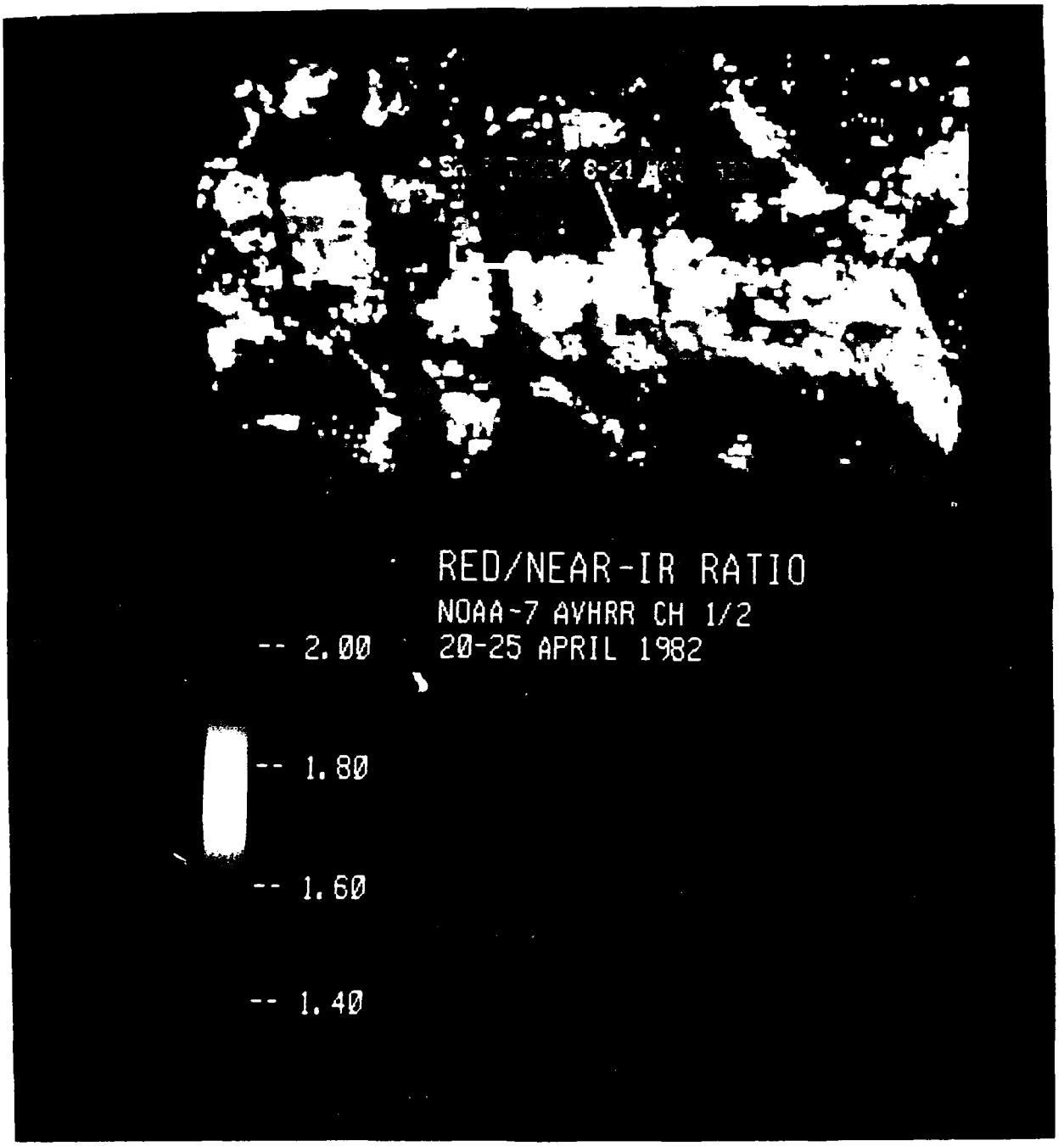

Fig. 4.2 Satellite radiance ratio 20-25 April 1982.

equatorial region. The higher values indicate a higher reflectance at the shorter wavelength of 0.63 μm (Ch1). This is because the computed reflectance is mostly attributed to scattering and an increase in Ch1 radiance would raise the Ch1/Ch2 ratio value. An elevated ratio indicates smaller sized particles in the distribution and is reflected in a greater slope in the dn/dr versus r relationship (Fig. 2.5c). As described by Charlson et al. (1987), high oceanic DMS relates to raised numbers of smaller aerosol particles. These smaller aerosol particles are inferred in satellite data with the relatively high ratio values.

Over latitudes greater than 10° north and south, ratio values are smaller than equatorial values. Reduced ratio values indicate lower Ch1 reflectance relative to Ch2. In this environment, the quantity of small particles in the atmosphere available to participate in a scattering event is less. A reduction in small aerosol particles should relate to depressed oceanic DMS values. As shown in Table 1 these values are in fact three times less than DMS measurements closer to the equator. This is consistent with observations made by Clarke et al., (1987), that equatorial oceanic DMS measurements were three to five times higher than average concentrations seen in the North Pacific Ocean from approximately 10°N to 45°N. The North Pacific Ocean is noted for its reduced productivity (Gross, 1972).

Fig. 4.2 also shows several regional maxima of Ch1/Ch2 ratio values. The western coast of the United States displays elevated Ch1/Ch2 ratio values of 2.0 or greater indicating the effects of urban aerosols from three major cities, namely Los Angeles, San Francisco

and Seattle. This location is also known for high rates of photosynthetic activity from nutrient rich upwelled waters. Similar values are evident over the western coastal boundaries of South America. Ratio values approximating 2.0 are recorded off the northwest corner of Australia. This local minimum is offshore from a major mining facility. Lastly, there is a patch of localized aerosol particles located east of Japan. A dust outbreak from the Gobi Desert and transport from urban centers is thought to be the cause of high ratio values there.

Perhaps the most striking observation from Fig. 4.2 is the geographic location of the ship crossing into higher Ch1/Ch2 ratio values. This latitude is approximately 6°N, precisely the latitude of the three fold increase of oceanic DMS from 50 to 120 ng DMS/l. The ratio values correlates well with high values of DMS maintained throughout the equatorial region, except for several local minimums. The Ch1/Ch2 ratio minimum is seen in the region south of the Marshall Islands during the last leg of the cruise.

To understand the oceanic DMS and Ch1/Ch2 ratio correlation more clearly, these parameters are plotted against each other (Fig. 4.3). A regression analysis using the method of least squares was performed on the data pairs. The straight line function that best fits the data is shown on the plot. The analysis shows that the data are correlated at the 95% confidence level with a correlation coefficient $r = 0.52$ using 61 samples. However, a large portion of the variability is not explained by the regression. This is probably related to other processes occurring coincident with particle formation such as

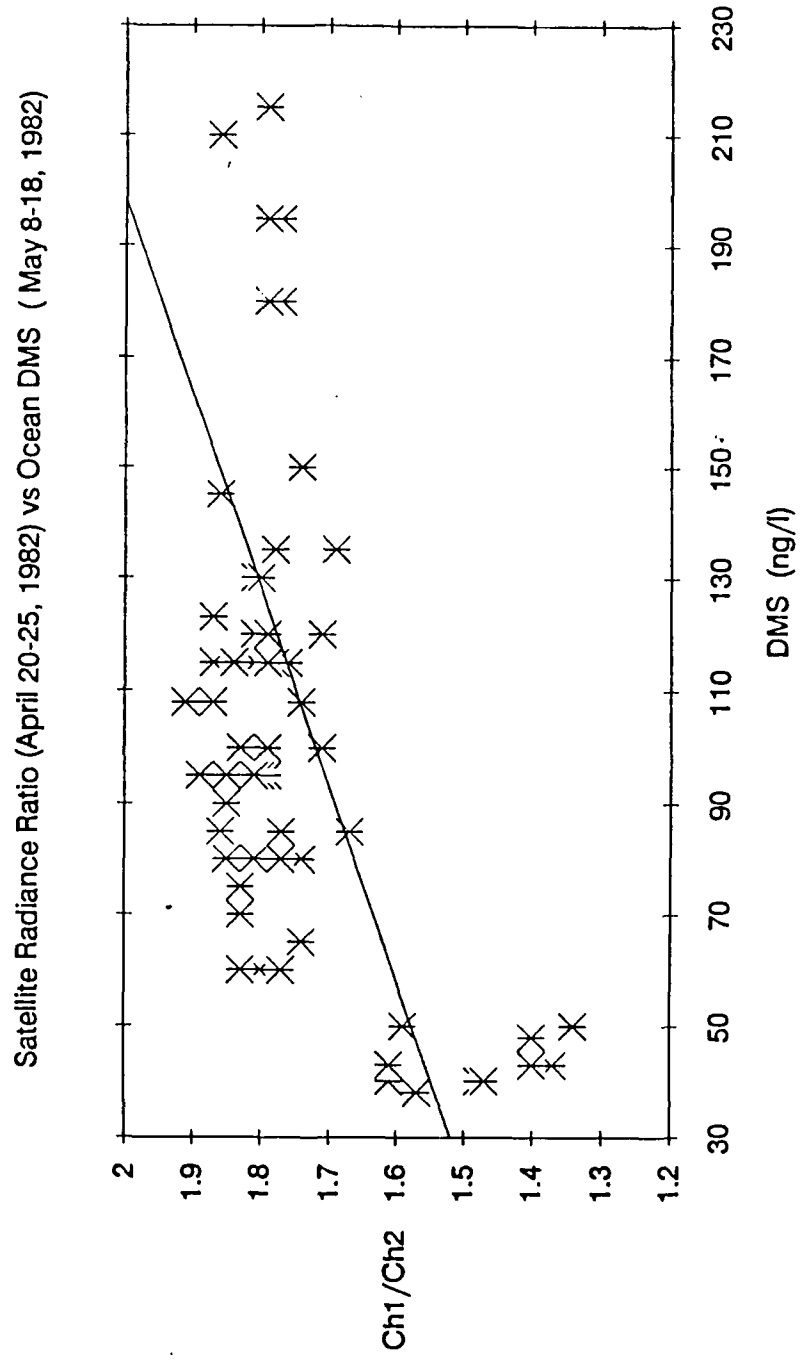

Fig. 4.3 Satellite radiance ratio (20-25 April 1982) vs. oceanic DMS (8-18 May 1982).

advection by persistent trade winds, air-sea interactions and DMS flux mechanisms not yet fully understood. In spite of this, a definite positive trend is observed; that is, Ch1/Ch2 ratio values increase with oceanic DMS. This is consistent with smaller aerosol particle size distribution as DMS levels in the ocean increase.

Further support for the DMS and Ch1/Ch2 relationship is seen in the 9-12 May image (Fig. 4.4). The ship track is again outlined in white. Satellite data for the entire geographical area were available during May. Therefore, the complete ship track is not presented. Note that the ratio values are approximately 0.2 units less than those observed for the April image. The reduction reflects the change in the processing algorithm which removes the path added radiance due to Rayleigh scattering and absorption due to ozone. The effect is thought to be about 10% of the values presented.

As in the April time period a maximum in ratio values is observed near 6°N. The raw data are displayed in Table 1. There are less data than the April image because satellite data for the entire shiptrack are not available.

DMS concentrations are plotted against Ch1/Ch2 ratios in Fig. 4.5. At 95% confidence the correlation is slightly less than the April data at $r = 0.46$ for $N = 50$ samples. An increase in the Ch1/Ch2 ratio to the north of 6°N without a corresponding increase in DMS is a possible explanation for the reduced correlation. However, a positive correlation exists between oceanic DMS concentration and Ch1/Ch2 ratio value.

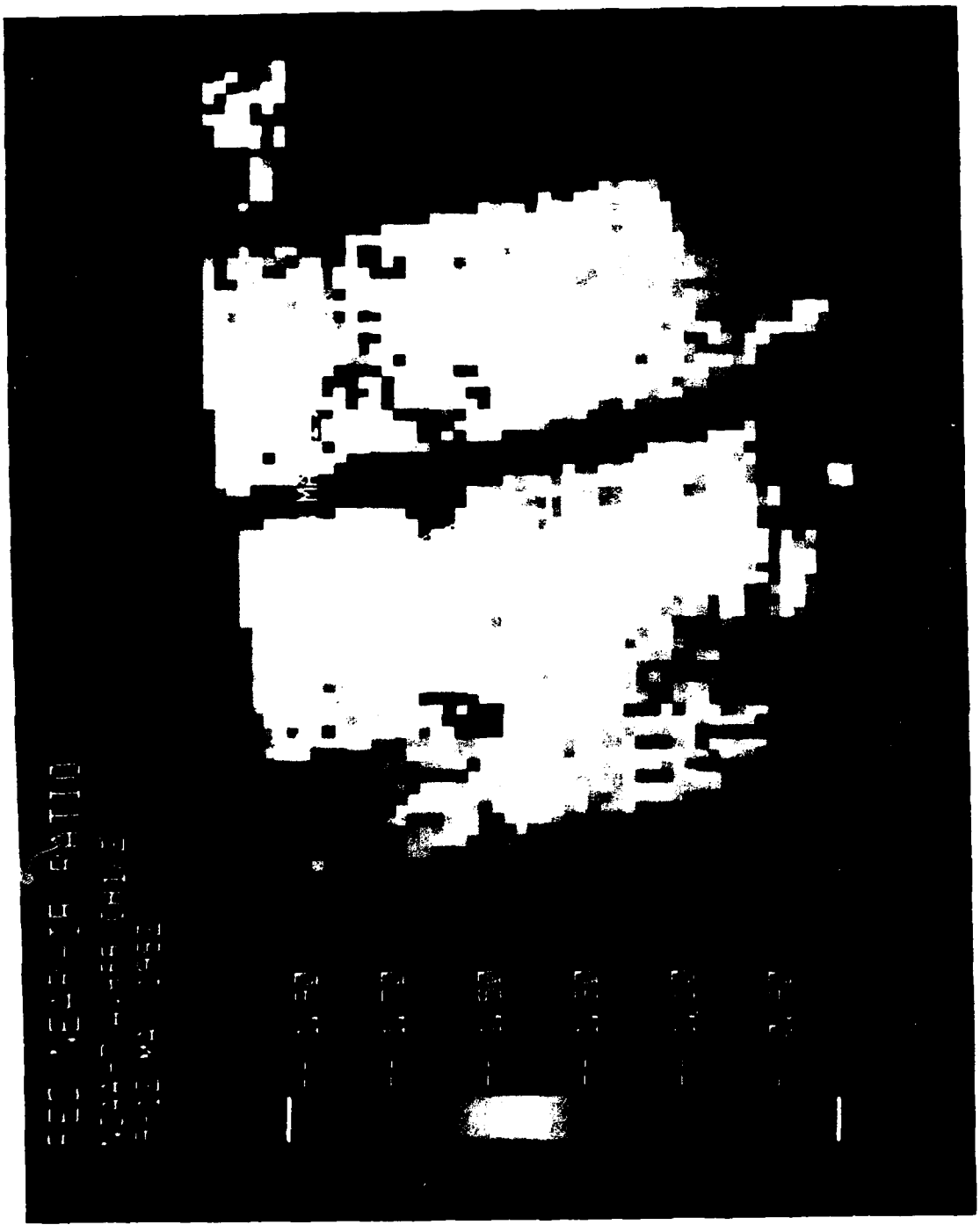

Fig. 4.4 Satellite radiance ratio from 9-12 May 1982.

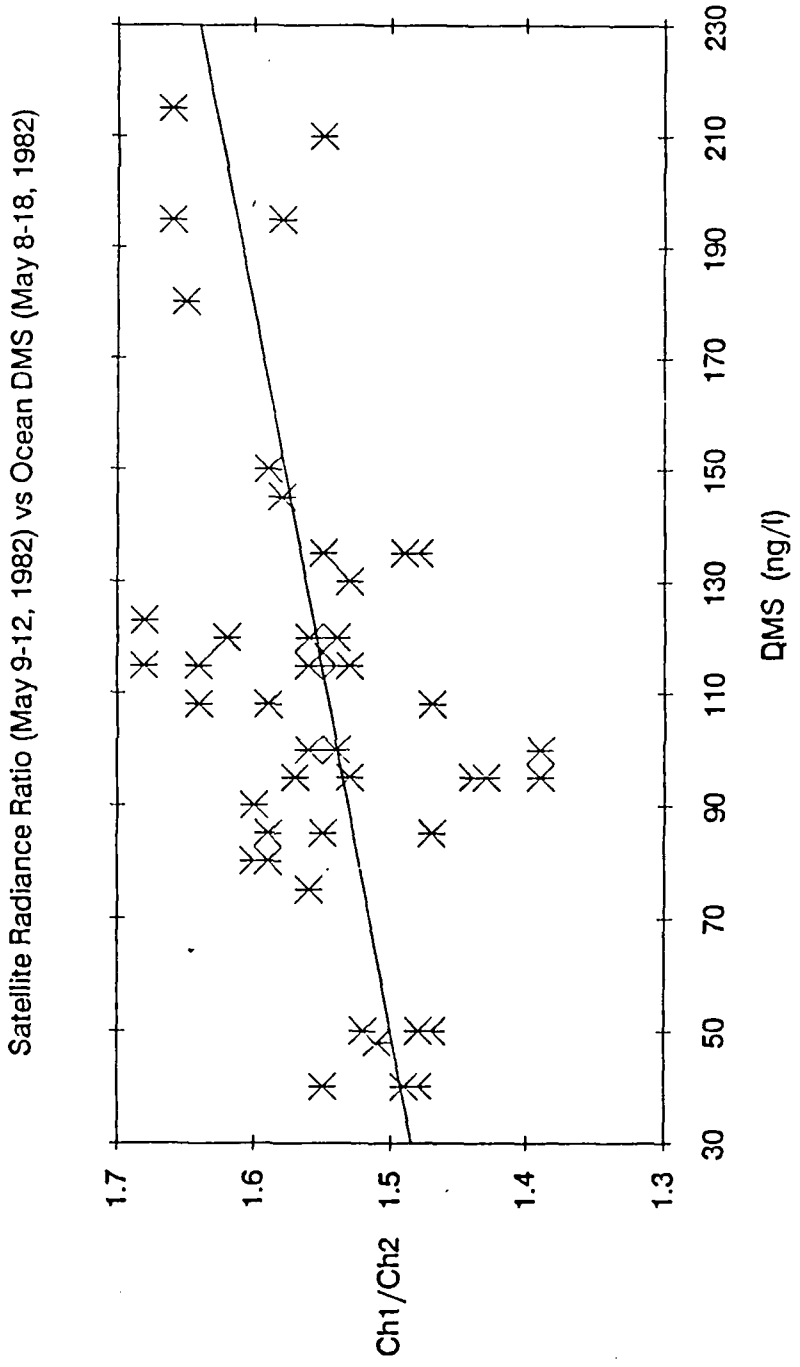

Fig. 4.5 Satellite radiance ratio (9-12 May 1982) vs. oceanic DMS (8-18 May 1982).

Atmospheric DMS and resulting particles are displaced due to the prevailing winds. The averaging area is roughly 100 km by 100 km. Therefore, advection of aerosol particles will affect the correlation provided the wind speed is large enough to move the aerosol approximately 100 km or more from the ocean source, roughly the resolution of the satellite data. The observed trade winds during the sampling period varied from the northeast to southeast. Wind speeds were typically 12-15 kt. Northeasterlies generally had higher velocities, while the winds with a southern component were of lesser velocity. The first two days saw the strongest winds with a maximum of 26 kt from the northeast. North of and along the equator, the winds were generally east to southeast at approximately 15 kt. Calm winds were noted along the equator at 160.8°W to 163.1°W (Table 1). The winds may play an advective role in transporting atmospheric DMS out of the region. The result is that wind advection should decrease the potential correlation between oceanic DMS and Ch1/Ch2 ratio values.

An additional parameter available in this data set that can be compared to oceanic DMS is sea-surface temperature. Fig. 4.6 displays the two variables. The correlation on the 52 samples is $r = 0.43$. Only 20% of the variability is explained by the regression. However, the correlation is significant meaning that a rise in sea surface temperature corresponds to a rise of some magnitude in oceanic DMS. The correlation may be coincident. Processes that may be dependent upon temperature, such as DMS production rates, atmospheric

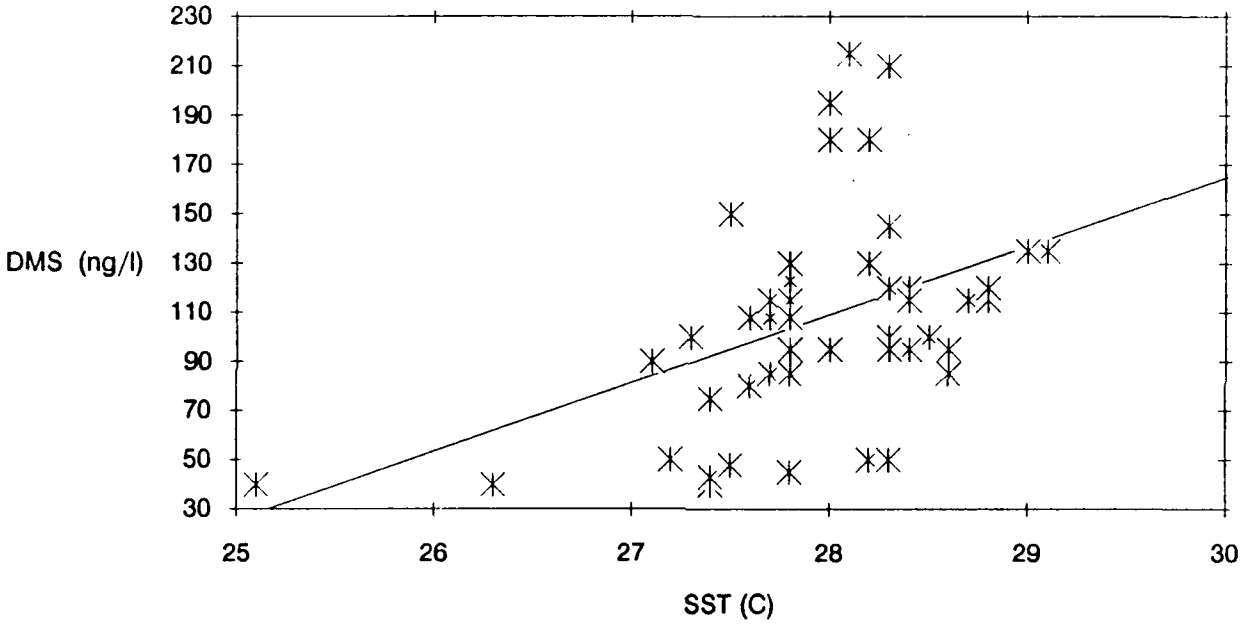

Fig. 4.6 Oceanic DMS vs. sea-temperature (8-18 May 1982).

ventilation and phytoplankton productivity could be affected by varying water masses.

V. CONCLUSIONS AND RECOMMENDATIONS

Aerosol characteristics inferred from AVHRR data were compared with sea-surface measurements of DMS in the central equatorial North Pacific Ocean. Ch1/Ch2 ratio values were used as a tool to detect variations of aerosol particle size distribution. The detected upwelled radiance from AVHRR Ch1 (0.63 μm) and Ch2 (0.86 μm) was evaluated by applying accepted assumptions to the radiative transfer equation (RTE). Using the radiation transfer equation, procedures developed at the Naval Postgraduate School were used to process the satellite data. Two climatological algorithms produced Ch1/Ch2 ratio images from AVHRR data from April and May 1982. The first algorithm was developed by Pfeil (1986) and applied to the April data. Cloud contaminated pixels were eliminated and only cloud free pixels were used to produce a Ch1/Ch2 ratio image. Frost (1988) improved the original algorithm in two ways. First, the path added effects for Rayleigh scattering and absorption effects of ozone were removed. This resulted in ratio values about 0.2 units less than those observed in Pfeil (1986). Second, a better check for contaminated pixels provided data that was eliminated. Pfeil (1986) method was more conservative and deleted more cloudless pixels.

The Ch1/Ch2 ratio values were compared with seventy surface oceanic DMS measurements taken by the R/V DISCOVERER from 8-21 May 1982. The analysis shows that gradients in oceanic DMS concentrations are related to variations in atmospheric aerosol particle size

distributions. As hypothesized by Charlson et al. (1987), this would imply bio-regulation of the global climate is possible because DMS is found throughout the world's oceans.

In this study, we also observed a slight positive correlation between sea-surface temperature and waterborne DMS. This suggests that elevated ocean temperatures provide a more favorable environment for DMS transport. Also, DMS production rates may be greater at higher ocean temperatures. Further, the phytoplankton species distribution varies with their environmental temperatures.

Varying the atmospheric aerosol particle size distribution affects CCN population. In response, cloud albedo is modified. The earth's temperature is sensitive to cloud albedo. Therefore, global climate may be altered by oceanic DMS production, which is transported to the atmosphere and converted to aerosol particles. The presented evidence supports the Charlson et al. (1987) hypothesis that global climatic change can be regulated through biological feedback mechanisms controlling cloud albedo.

The mechanisms within the climatic feedback loop are complicated processes. They are not well understood and additional research is required. We need to understand variations in phytoplankton taxonomy. In some situations, chlorophyll-a is related to DMS, however, not all phytoplankton are DMS producers. Also, algae rarely produce DMS at the same rate. We also need to learn the factors that affect oceanic DMS emissions to the atmosphere. It is unclear as to exactly what climatic factors are involved in DMS ventilation across the air-sea interface. The climatic response, by changing cloud albedo, may have

a positive or negative affect on DMS production. A positive response would result in climate regulation. This is the most uncertain part of the feedback loop.

Lastly, we need to more accurately quantify the relationship between oceanic DMS concentration in the air and populations of CCN. It is suspected that increases in oceanic DMS transport into the atmosphere would elevate the CCN population. Analysis of the new in-situ data will hopefully provide additional support for the climatic feedback hypothesis.

LIST OF REFERENCES

Andreae, M.O., and H. Raendonck, 1983: Dimethylsulfide in the surface ocean and the marine atmosphere; A global view, Science, **221**, 744-747.

Barnard, W.R., M.O. Andreae, W.E. Watkins, H. Bingemer, and H.W. Georgi, 1982: The flux of dimethylsulfide from the oceans to the atmosphere, J. Geophys. Res., **87(C11)**, 8787-8793.

Bohren, C.F. and D.R. Huffman, 1983: Absorption and Scattering of Light by Small Particles. John Wiley and Sons, New York, 530 pp.

Bulfinch, S.R., 1986: Determination of the atmospheric aerosol distribution by multi-channel remote sensing techniques. M.S. Thesis, Naval Postgraduate School, Monterey, CA, 89 pp.

Charlson, R.J., J.E. Lovelock, M.O. Andreae, and S.G. Warren, 1987: Oceanic phytoplankton, atmospheric sulphur, cloud albedo and climate. Nature, **326**, 655-661.

Clarke, A.D., N.C. Ahlquist, and D.S. Covert, 1987: The Pacific marine aerosol: Evidence for natural acid sulfates, J. Geophys. Res., 92(D4), 4179-4190.

Cline, J.D., and T.S. Bates, 1983: Dimethyl sulfide in the equatorial Pacific Ocean: A natural science of sulfur to the atmosphere, Geophys. Res. Letters, **10**, 949-952.

Durkee, P.A., 1984: The relationship between marine aerosol particles and satellite-detected radiance. Ph.D. Thesis, Colorado State University, Fort Collins, Colorado, US ISSN 0067-0340, 124 pp.

Durkee, P.A., D.R. Jensen, E.E. Hindman, and T.H. Vondor Harr, 1986: The relationship between marine aerosol particles and satellite-detected radiance. J. Geophys. Res., **91(D3)**, 4063-4072.

Fleagle, R.G. and J.A. Businger, 1980: An Introduction to Atmospheric Physics, (Second Edition). Academic Press, Inc., Orlando, FL, 432 pp.

Frost, E.M., 1988: Global scale estimates of aerosol particle characteristics. M.S. Thesis, Naval Postgraduate School, Monterey, CA, 54 pp.

Griggs, M., 1975: Measurements of atmospheric aerosol optical thickness over water using ERTS-1 data, J. Air. Pollut. Control Assoc., 25, 622-626.

Griggs, M., 1983: Satellite measurements of tropospheric aerosols. Adv. Space Res., 2(5), 109-118.

Gross, M.G., 1972: Oceanography-a view of the earth. Prentice-Hall, New Jersey, 497 pp.

Gruber, A., I. Ruff, and C. Earnest, 1983: Determination of the planetary radiation budget from TIROS-N satellites. NOAA Technical Report, NESDIS 3, Washington, DC, 12 pp.

Hanel, G., 1976: The properties of atmospheric aerosol particles as functions of the relative humidity at thermodynamic equilibrium with the surrounding moist air. In Advances in Geophysics, 19, edited by H.E. Landsberg and J. Van Mieghen, Academic Press, New York, 73-188.

Hobbs, P.V., H. Harrison, and E. Robinson, 1974: Atmospheric effects of pollutants. Science, 183, 909-915.

Liou, K.N., 1980: An introduction to atmospheric radiation. Academic Press, New York, 392 pp.

McMormick, R.A., J.H. Ludwig, 1967: Climate modification by atmospheric aerosols. Science, 156, 1358-1359.

Pfeil, F.R., 1986: Developing a physical basis for an aerosol climatology of the Pacific Ocean. M.S. Thesis, Naval Postgraduate School, Monterey, CA, 75 pp.

Pruppacher, H.R., and J.D. Klett, 1978: Microphysics of Clouds and Precipitation. Reidel, Dordrecht, 398 pp.

Ramsey, R.C., 1968: Study of the remote measurement of ocean color. Final report, TRW, NASW-1658.

Shettle, E.P. and R.W. Fenn, 1979: Models for the aerosols of the lower atmosphere and the effects of humidity on their optical properties. Tech. Rep. AFGL-TR-79-0214, Air Force Geophys. Lab., Hanscomb Air Force Base, MA.

Twomey, S., 1977: Atmospheric Aerosols. Elsevier, Amsterdam.

World Climate Research Programme, 1986: A preliminary cloudless standard atmosphere for radiation computation. WCP-112, WMO/TD-No. 24.

INITIAL DISTRIBUTION LIST

		No. Copies
1.	Defense Technical Information Center Cameron Station Alexandria, VA 22304-6145	2
2.	Library, Code 0142 Naval Postgraduate School Monterey, CA 93943-5002	2
3.	Chairman (Code 68Co) Department of Oceanography Naval Postgraduate School Monterey, CA 93943-5004	1
4.	Chairman (Code 63Rd) Department of Meteorology Naval Postgraduate School Monterey, CA 93943-5004	1
5.	Prof. P. A. Durkee (Code 63De) Department of Meteorology Naval Postgraduate School Monterey, CA 93943-5004	11
6.	Prof. C. H. Wash (Code 63Wx) Department of Meteorology Naval Postgraduate School Monterey, CA 93943-5004	1
7.	LCDR Richard A. Shema, USN COMNAVOCEANCOM/JTWC COMNAVMARIANAS Box 12 FPO San Francisco, CA 96630-2926	4
8.	Director Naval Oceanography Division Naval Observatory 34th and Massachusetts Avenue NW Washington, DC 20390	1
9.	Commander Naval Oceanography Command NSTL Station Bay St. Louis, MS 39522	1

10. Commanding Officer 1
Naval Oceanographic Office
NSTL Station
Bay St. Louis, MS 39522

11. Commanding Officer 1
Fleet Numerical Oceanography Center
Monterey, CA 93943

12. Office of Naval Research (Code 420) 1
800 N. Quincy Street
Arlington, VA 22217

13. Commanding Officer 1
Naval Environmental Prediction Research Facility
Monterey, CA 93943

14. Chairman, Oceanography Department 1
U.S. Naval Academy
Annapolis, MD 21402

15. Scientific Liaison Office 1
Office of Naval Research
Scripps Institution of Oceanography
La Jolla, CA 92037